ACS OMEGA

http://pubs.acs.org/journal/acsodf

Article

Mesoporous Carbon/α-Fe_2O_3 Nanoleaf Composites for Disposable Nitrite Sensors and Energy Storage Applications

Palani Barathi,* Anthonisamy Devaraj, and Angaiah Subramania*

Cite This: *ACS Omega* 2020, 5, 32160−32170

Read Online

ACCESS | Metrics & More | Article Recommendations | Supporting Information

ABSTRACT: In this work, we report a novel hydrothermal synthesis of α-Fe_2O_3 nanoleaf-incorporated mesoporous carbon-chitosan (α-Fe_2O_3@MPC-chit) as a versatile disposable sensor for selective electrochemical detection of nitrite and for supercapacitor applications. The newly synthesized α-Fe_2O_3@MPC-chit nanocomposite was characterized by scanning electron microscopy, X-ray diffraction, Fourier transform-infrared spectroscopy, UV, and Raman spectroscopy. The extensive physicochemical characterization reveals the strong immobilization of α-Fe_2O_3 nanoleaves within the MPC-chit composite. The electrochemical characterization with cyclic voltammetry and impedance spectroscopy using $[Fe(CN)_6)]^{3-/4-}$ as a redox probe concludes good electron conductivity and efficient electron transfer behavior of α-Fe_2O_3@MPC-chit. The α-Fe_2O_3@MPC-chit modified electrode exhibits excellent electrocatalytic activity toward nitrite oxidation. The amperometric method of nitrite detection showed a linear range of up to 200 μmol L^{-1}. The current sensitivity and detection limit were found to be 0.913 μA μM^{-1} and 31 nM cm^{-2}, respectively. The improved catalytic activity of the proposed electrode was endorsed by the synergistic effect of α-Fe_2O_3 with the MPC-chit composite. The ability of the proposed electrode was demonstrated by the successful detection of nitrite present in tap water, river water, and industrial samples with extensive recovery values. Furthermore, the α-Fe_2O_3@MPC-chit modified stainless-steel electrode showed high-performance supercapacitor application and exhibited a large specific capacitance of 380 F g^{-1} at 1 A g^{-1}.

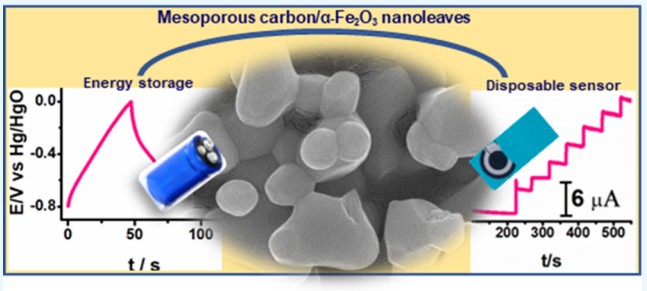

INTRODUCTION

The nanostructured hematite (α-Fe_2O_3) is a prominent kind of transition metal oxide, enabling its application in biosensors, drug delivery, optical devices, catalysts, pigments, electrode materials, gas sensors, supercapacitors, electromagnetic devices, and energy storage applications.[1−4] There are numerous methods adapted to synthesize iron oxides such as solvothermal, hydrothermal, coprecipitation, electron beam deposition, and electrochemical deposition.[5−8] In most of the synthetic procedures, iron(III) and iron(II) chloride were utilized as iron-containing precursors to prepare iron oxide, which are deliquescent (easily decompose in moist air) and expensive chemicals, respectively. Herein, we report the synthesis of nanostructured iron oxide using affordable potassium ferricyanide as a precursor through the hydrothermal method. The synthesized α-Fe_2O_3 nanoleaves were characterized and confirmed with basic techniques such as X-ray diffraction (XRD), Fourier transform infrared (FT-IR), Raman spectroscopy, and scanning electron microscopy (SEM). However, α-Fe_2O_3 nanoleaves themselves may not act as excellent candidates because they can irreversibly adsorb on the solid electrode surface which limits their application in energy storage and electrochemical sensors. Hence, it is important to rationally couple the α-Fe_2O_3 nanoleaves with other nanomaterials to form a novel hybrid structure which can reveal enhanced electrochemical activity. There have been recent reports on hybrid α-Fe_2O_3 composites such as graphene oxide-α-Fe_2O_3, MWCNT-α-Fe_2O_3, chitosan-α-Fe_2O_3-terephthalaldehyde, and carbon nitride-α-Fe_2O_3 used for electrochemical sensing of hydroquinone, ascorbic acid, DNA, and glucose, respectively.[9−12] Meanwhile, reduced graphene oxide-Fe_2O_3, *N*-RGO-Fe_2O_3, and single-crystalline Fe_2O_3 particles/graphene modified composites were reported for supercapacitor applications.[12−16] To the best of our knowledge, this is the first report on an α-Fe_2O_3 nanoleaf-decorated MPC-chit modified composite for two different potential applications: selective electrochemical sensing of nitrite at neutral pH and high-performance supercapacitor applications at alkaline pH. Recently, mesoporous carbon has attracted much attention as a host material for metals, metal oxides, and polymers for electrochemical sensors and energy storage applications.[17−19] The high surface area, good electrical

Received: June 1, 2020
Accepted: November 5, 2020
Published: December 7, 2020

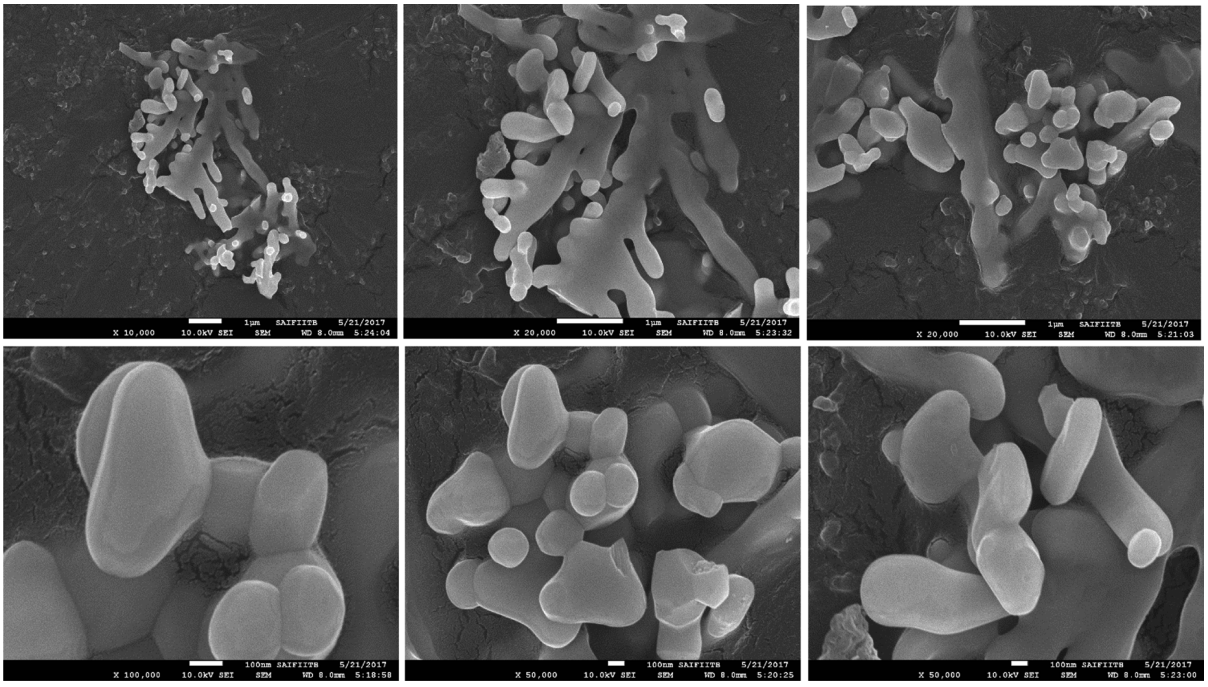

Figure 1. FESEM images of α-Fe_2O_3 nanoleaves at different magnifications.

conductivity, a well-defined, large pore volume, and the unique features resulting from combining biopolymer chitosan enable higher α-Fe_2O_3 nanoleaf incorporation for improved electrocatalytic activity of nitrite and supercapacitor applications.

Nitrite has been commonly used as a food additive, corrosion inhibitor, and fertilizing agent.[20] On the other side, it is known as a natural environmental pollutant and human carcinogen.[21] Especially, nitrite concentration is increasing in water sources because of its vast usage in agriculture and industries. Excess concentration of nitrite in the human body can irreversibly bind with hemoglobin and form methemoglobin, which hinders the oxygen transport capability of blood. Therefore, it is extremely important to the accurate and rapid detection of nitrite in biological and environmental water samples. As of now, various analytical techniques have been explored for accurate detection of nitrite including high-performance liquid chromatography (HPLC), spectroscopy, capillary electrophoresis, fluorescence, and chemiluminescence.[22−25] Unfortunately, the aforementioned techniques suffered from extensive sample preparation, expensive instrumentation, low specificity, time-consuming process, and inability of direct detection. Although electrochemical techniques possess several advantages including simple operation, low cost, versatility, high sensitivity, selectivity, and a wide linear range over conventional routine techniques. However, the detection of nitrite at a bare (unmodified) electrode is limited with a large overpotential, leading to poor selectivity against common interfering chemicals.[26] Moreover, the oxidized product of nitrite and intermediate species can irreversibly bind with traditional solid electrodes, leading to poor sensitivity and reproducibility.[26] To overcome this issue, Compton et al. developed an effective ultrasonication method for cleaning the electrode surface.[27] Hence, constructing an excellent modified electrode with high sensitivity and selectivity at a low detection potential at neutral pH is the key problem for researchers for detecting nitrite. There are various chemically modified electrodes reported recently such as polymers, metal nanoparticles (MNPs), metal oxide nanoparticles, phthalocyanines, chalcogenides, carbon ink, and thiazine metachromatic dye for selective electrochemical detection of nitrite.[28−37] Nevertheless, most of the modified electrodes have serious issues including instability at neutral pH, poor sensitivity, and a detection limit which hinders their extension to real-time applications.[38−41] For instance, $PrFeO_3$−MoS_2 nanosheets,[31] graphene−polypyrrole−chitosan,[30] graphene−AuNPs,[29] and metal−organic-gels−bis-(benzimidazole) ligands−copper-35 modified electrodes showed either poor sensitivity or short linear range in acidic medium. Herein, we report α-Fe_2O_3-decorated mesoporous carbon−chitosan composite (α-Fe_2O_3@MPC-chit) modified screen-printed electrodes for highly sensitive and selective electrochemical detection of nitrite in a pH 7 phosphate-buffered solution (PBS).

A developed nanostructured α-Fe_2O_3@MPC-chit modified composite showed highly sensitive and selective amperometric sensing of nitrite in pH 7 PBS and an excellent supercapacitor characteristic behavior over the recently reported α-Fe_2O_3 modified systems. The enhanced sensitivity and supercapacitor features could be accredited to the stable immobilization of α-Fe_2O_3 within the MPC-chit nanocomposite. The developed detector was further utilized for amperometric sensing of nitrite in three different environmental samples with satisfactory recovery values.

RESULTS AND DISCUSSION

Physicochemical Characterization of the Synthesized α-Fe_2O_3 Nanoleaves. At first, the morphology of the synthesized α-Fe_2O_3 nanoparticle (NP) was investigated by SEM (Figure 1). It displays that the synthesized α-Fe_2O_3 NP consists of an agglomerated leaf-shaped species with a uniform size. UV spectra for the as-synthesized α-Fe_2O_3 nanoleaves were recorded. As shown in Figure S1, a broad spectrum in the region of 200−800 nm having a maximum at 308 nm corresponding to direct ligand−metal transitions (O^{2-} 2p →

https://dx.doi.org/10.1021/acsomega.0c02594
ACS Omega 2020, 5, 32160−32170

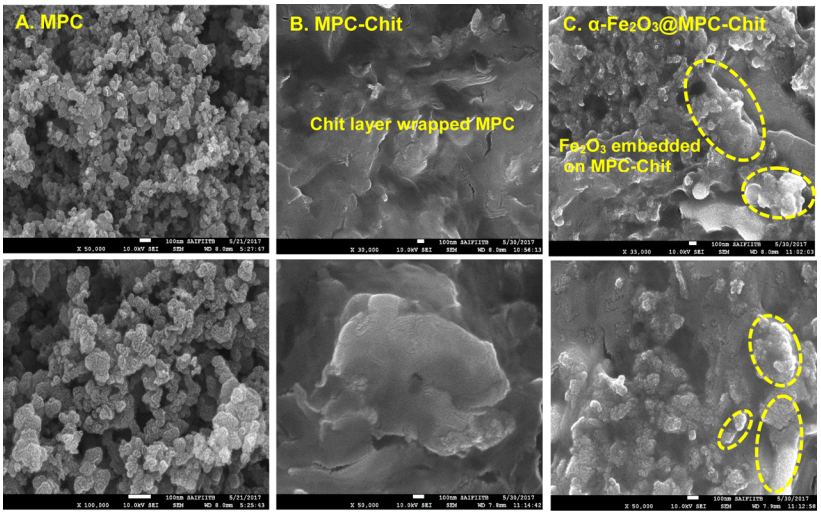

Figure 2. FESEM images of MPC (A); MPC-chit (B); and α-Fe_2O_3@MPC-chit (C).

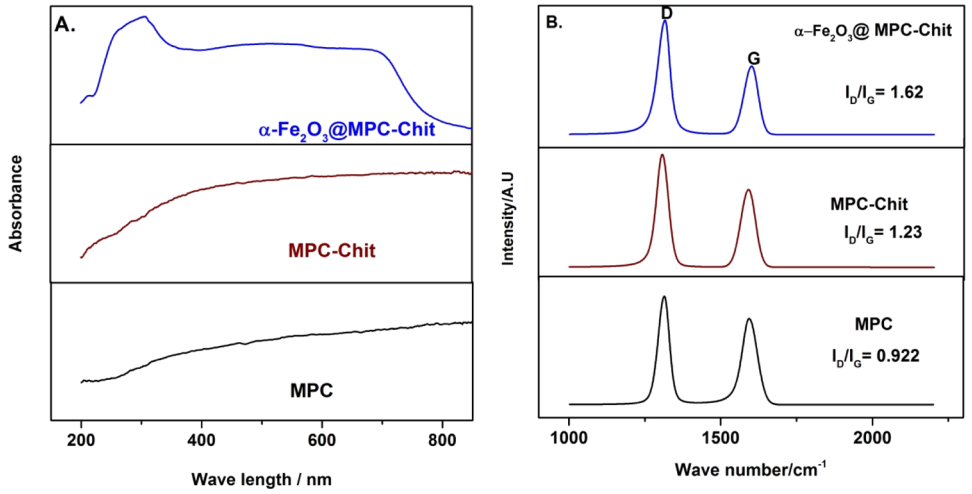

Figure 3. UV (A) and Raman spectra (B) of MPC; MPC-chit; and α-Fe_2O_3@MPC-chit.

Fe^{3+} 3d) and that at 690 nm corresponding to indirect metal−metal transitions (Fe^{3+} 3d → Fe^{3+} 3d) were observed in the UV and visible region, respectively. The observed absorption bands are in good agreement with the literature report.[42,43] FT-IR spectroscopy is a powerful technique to identify Fe_2O_3. FT-IR spectra of the as-prepared α-Fe_2O_3 nanoleaves are shown in Figure S2. The sharp and intense peaks have appeared at 450 and 532 cm^{-1}, which are in good agreement with Fe−O stretching and bending vibrations of α-Fe_2O_3 NPs.[3,4] The structure and crystallinity of the synthesized α-Fe_2O_3 nanoleaves were characterized by powder XRD and the results are shown in Figure S3. The XRD pattern of the as-prepared α-Fe_2O_3 nanoleaves displayed several diffraction peaks at 2θ = 24.2, 33.1, 35.8, 40.9, 49.7, 54.3, 57.7, 62.4, 64.1, and 72.2° indexed to (012), (104), (110), (113), (024), (116), (018), (214), (300), and (1010), respectively. The obtained diffraction patterns are strong and sharp, suggesting strong crystallinity of the prepared samples, and they are unambiguously indexed with a rhombohedral phase of a hematite structure (α-Fe_2O_3 nanoleaves).[3,4,44] Furthermore, the quality of the crystalline samples and structures was characterized by nondestructive confocal Raman spectroscopy. As shown in Figure S4, seven distinct and sharp lines, namely, two A_{1g} modes (225 and 495) and five E_g (244, 292, 299, 408, and 609) modes were observed in the Raman spectrum, indicating a D_{3d}^6 crystal space group of a hematite phase.[3,4,44] All these results concluded that α-Fe_2O_3 nanoleaves were successfully synthesized with a simple preparation procedure.

Physicochemical Characterization of the α-Fe_2O_3@MPC-chit Nanocomposite. The morphology of MPC, MPC-chit, and α-Fe_2O_3@MPC-chit was characterized by SEM (Figure 2). The SEM image of MPC displayed a uniform arrangement of porous carbon species, whereas MPC-chit showed a flat sheet-like structure without any mesoporous shape, suggesting that MPC was completely dispersed in the chit solution. On the other hand, α-Fe_2O_3 nanoleaves were uniformly distributed within the MPC-chit composite, as shown in Figure 2C. The SEM morphologies confirm successful immobilization of α-Fe_2O_3 nanoleaves on MPC-chit composites. The UV spectrum of MPC, MPC-chit, and α-Fe_2O_3@MPC-chit is shown in Figure 3A α-Fe_2O_3@MPC-chit displays similar UV patterns obtained for α-Fe_2O_3 nanoleaves (Figure S1), whereas no specific absorption patterns were observed for MPC and MPC-chit composites. This observation implies a strong interaction of the as-prepared α-Fe_2O_3 nanoleaves with MPC-chit. Raman spectroscopy is a powerful

https://dx.doi.org/10.1021/acsomega.0c02594
ACS Omega 2020, 5, 32160−32170

nondestructive technique for the characterization of the carbon-based material. Raman spectra of MPC, MPC-chit, and α-Fe_2O_3@MPC-chit are shown in Figure 3B. All spectra comprise two sharp peaks at 1306 and 1591 cm^{-1} associated with D and G band, respectively. The D band is related to a disordered sp^3 amorphous carbon which may be because of the finite particle size effect, structural defect, and lattice distortion, and the G band originates from a pure graphitic sp^2 carbon. The relative intensity between D and G (I_D/I_G) indicates the measure of disordered graphite.[45] The calculated I_D/I_G value for MPC is 0.922. The I_D/I_G ratio increases after the dispersion of MPC in the chit solution, and it was further increased by incorporating the α-Fe_2O_3 nanoleaves into MPC-chit. This observation indicates that the as-prepared α-Fe_2O_3 nanoleaves were successfully immobilized into the MPC-chit composite. Furthermore, it was confirmed by FT-IR spectroscopy. Figure 4 shows the FT-IR spectra of MPC, MPC-chit, and α-Fe_2O_3@MPC-chit. As shown in Figure 4, the spectra show a common absorption peak at ~1025 cm^{-1}, which indicates a =C−H in-plane deformation of MPC. The absorption spectrum located in the region of 1400−1600 cm^{-1} represents the amide bands of the chit layer in the MPC-chit composite, as shown in Figure 4B. The α-Fe_2O_3@MPC-chit shows distinct peaks at 450 and 532 cm^{-1}, which is the Fe−O bond vibration, in addition to the pattern of MPC and chit.[3,4,44] These results confirm the strong immobilization of α-Fe_2O_3 nanoleaves into the MPC-chit composite.

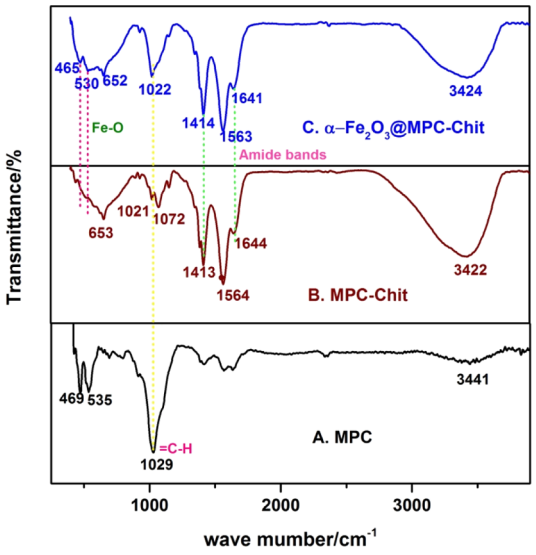

Figure 4. FT-IR responses of MPC (A); MPC-chit (B); and α-Fe_2O_3@MPC-chit (C).

Electrochemical Characterization of the α-Fe_2O_3@MPC-chit Modified Electrode. The electrochemical behavior of the modified electrodes was investigated by cyclic voltammetry (CV) using $[Fe(CN)_6)]^{3-/4-}$ as a benchmark redox system. Figure 5 shows the cyclic voltammograms of MPC-chit/SPCE- and α-Fe_2O_3@MPC-chit/SPCE modified electrodes in a 5 mM $[Fe(CN)_6)]^{3-/4-}$ dissolved KCl solution at a scan rate of 10 mV s^{-1}. As shown in Figure 5A, MPC-chit/SPCE showed a well-defined and sharp redox peak with a peak-to-peak separation ($\Delta E_p = E_{pa} - E_{pc}$) of 65 mV, whereas α-Fe_2O_3@MPC-chit/SPCE showed a relatively lower peak-to-peak separation (ΔE_p = 60 mV) with a higher redox peak current over the MPC-chit modified electrode. This observation concludes a good electron conductivity of $[Fe(CN)_6)]^{3-/4-}$ redox probes at the α-Fe_2O_3@MPC-chit/SPCE interface.

In general, the geometrical area (A_{geo}) of the electrode does not resemble the real electroactive area of the electrode (A_{real}). The Randles−Ševcik equation can be used to determine the true active area of the electrode using an electrochemical interfacial technique such as CV.[46]

$$I_{p,f}^{rev} = \pm 0.446\, nF A_{real} C \sqrt{n} F D v / RT \quad (1)$$

where, n is the number of electron transfer, $I_{p,f}$ is the forward peak current, F is the Faraday constant (C mol^{-1}), v is the voltammetric scan rate (V s^{-1}), R is the universal gas constant, T is the temperature in Kelvin, D is the diffusion coefficient (cm^2 s^{-1}), and A_{real} is the electroactive area of the electrode (cm^2). The calculated electroactive surface area of the MPC-chit/SPCE and α-Fe_2O_3@MPC-chit/SPCE is 0.06742 and 0.08630 cm^2, respectively. The ratio between the real and geometrical area specifies the measure of real percentage (% real = $(A_{real}/A_{geo}) \times 100$), which is found to be 95.36 and 122% for the MPC-chit/SPCE and α-Fe_2O_3@MPC-chit/SPCE, respectively. The increased real percentage confirms the higher α-Fe_2O_3 nanoleaf incorporation within the MPC-chit.

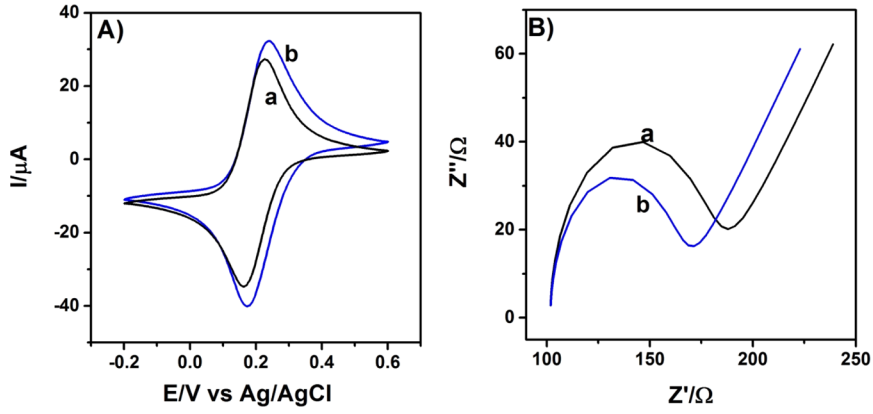

Figure 5. (A) CV response and (B) EIS behavior of (a) MPC-chit and (b) α-Fe_2O_3@MPC-chit in 0.1 M KCl containing 5 mM $[Fe(CN)_6]^{3-/4-}$ solution at an applied potential of 0.2 V vs Ag/AgCl.

https://dx.doi.org/10.1021/acsomega.0c02594
ACS Omega 2020, 5, 32160−32170

Electrochemical impedance spectroscopy (EIS) has been generally studied for understanding the electrode−electrolyte interface of modified electrodes. In general, the impedance spectrum consists of a semicircle and linear portions at higher and lower frequencies, respectively. The diameter of the semicircle portion is equal to the charge-transfer resistance (R_{CT}).[47] The EIS spectra of MPC-chit- and α-Fe_2O_3@MPC-chit modified electrodes are shown in Figure 5B. The diameter of a semicircle for α-Fe_2O_3@MPC-chit is quite less than that of the MPC-chit modified electrode, which implies the efficient electron transfer behavior of α-Fe_2O_3@MPC-chit. These observations agree with our CV results of $[Fe(CN)_6]^{3-/4-}$ redox probes.

Electrocatalytic Behavior of the α-Fe_2O_3@MPC-chit Modified Electrode. The direct electrochemical oxidation of nitrite was examined using MPC-chit and α-Fe_2O_3@MPC-chit modified screen-printed electrodes in the presence of 1 mM nitrite containing 0.1 M pH 7 PBS at a scan rate of 10 mV s^{-1} (Figure 6A). A well-defined oxidation peak at +0.94 V versus Ag/AgCl was observed for the MPC-chit modified electrode with a peak current of ∼12.3 μA (Figure 6A curve b). Still, the obvious anodic peak current at ∼24.7 μA with a low detection potential of 0.76 V was observed for the α-Fe_2O_3@MPC-chit, which implies that α-Fe_2O_3 nanoleaves were compactly incorporated within the MPC-chit, contributing a major catalytic role for the detection of nitrite (Figure 6A curve c). Note that the α-Fe_2O_3@MPC-chit/SPCE did not show any specific oxidation peak in the absence of nitrite (Figure 6A curve a), implying that the current response was not from the electrode materials; it is purely because of nitrite oxidation. Figure 6B shows the cyclic voltammograms obtained from α-Fe_2O_3@MPC-chit/SPCE modified electrodes at different concentrations of nitrite at a scan rate of 10 mV s^{-1}. As shown in the Figure, the anodic peak current of the α-Fe_2O_3@MPC-chit/SPCE modified electrode increases systematically with an increase in nitrite concentration in pH 7 PBS. The calibration plot of anodic peak current versus nitrite concentration is linear in the range of 0.25 to 12 mM and the sensitivity is calculated to be 31.46 μA mM^{-1} (Figure 6B Inset). The efficient nitrite catalytic activity of the modified electrode suggested that the as-prepared α-Fe_2O_3@MPC-chit nanocomposites can be a promising platform for the electrochemical detection of nitrite. Furthermore, the electrochemical behavior of the modified electrode toward nitrite detection was investigated by CV at different scan rates. The anodic peak currents increase gradually and the oxidation peak potential of nitrite shifts toward a positive direction with increasing scan rate from 5−200 mV s^{-1} (Figure 7A). The oxidation peak currents linear to the scan rate (v) as well as the square root of the scan rate and the regression coefficient are 0.99 and 0.97, respectively (Figure 7A Insets). These results imply that electrocatalytic oxidation of nitrite at α-Fe_2O_3@MPC-chit/SPCE involves both diffusion- and adsorption-controlled electron transfer processes. The positive shift in the oxidation peak potential with the scan rate is likely due to the adsorption of nitrite and its oxidation product at the α-Fe_2O_3@MPC-chit surface, which may limit the kinetics of the adsorption-controlled irreversible electrochemical reaction. The relationship between the E_{pa} and scan rates can be described by the Laviron equation.[48]

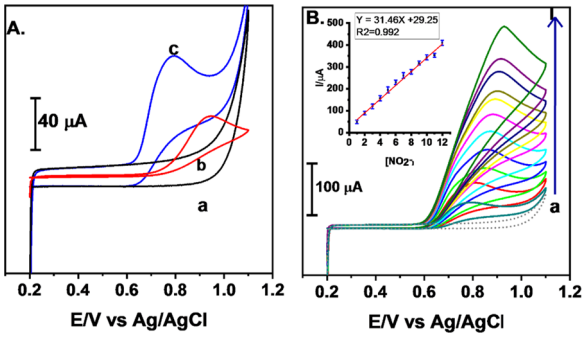

Figure 6. (A) CV responses for α-Fe_2O_3@MPC-chit without (a) and with (c) presence of 1 mM NO_2^-; CV response for MPC-chit in the presence of 1 mM NO_2^- (b); (B) CV responses for α-Fe_2O_3@MPC-chit modified screen printed electrodes upon successive addition of different concentrations of NO_2^- at a scan rate of 10 mV s^{-1} and its calibration plot (Inset B). Error bars denote standard deviation of three repeating measurements.

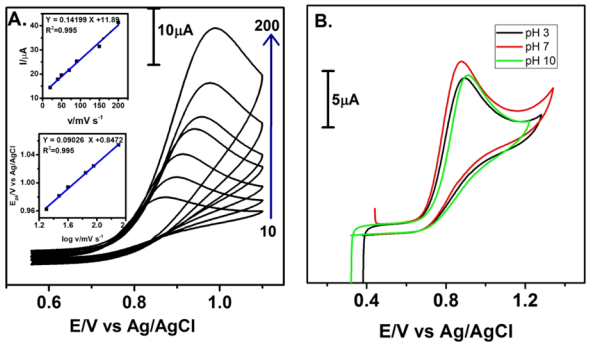

Figure 7. CV responses for different scan rates from 10−200 mV s^{-1} using α-Fe_2O_3@MPC-chit modified screen printed carbon electrodes containing 0.5 mM NO_2^- in pH 7 PBS (A); linear plot for scan rate vs I_{pa} of NO_2^- (Inset A). Effect of different pH solutions using α-Fe_2O_3@MPC-chit modified electrodes containing 0.5 mM NO_2 (B).

$$E_{pa} = E^0 + (RT/\alpha nF)\ln(RTk^0/\alpha nF) + (RT/\alpha nF)\ln v \quad (2)$$

where E^0 represents formal redox potential, α is the electron transfer coefficient, K^0 indicates a standard rate constant of surface reaction, n is the electron transfer numbers, and other parameters, R, T, v, and F have their usual meanings. The αn value can be calculated from the slope and intercept of the linear equation of E_{pa} versus scan rate (v). The value of α (assume that n is one for nitrite oxidation) was calculated to be 0.6, which indicates an irreversible electron transfer reaction. The effect of pH on nitrite detection at the α-Fe_2O_3@MPC-chit modified electrode was studied in the pH range of 3 to 10 (Figure 7B). It was found that there was no obvious variation in the nitrite oxidation peak potential and current with increasing pH of the solution from 3 to 10, which indicates an excellent electrochemical activity and proton independent catalytic activity of the α-Fe_2O_3@MPC-chit modified electrode toward nitrite detection and can be used for wider pH ranges. For practical application, pH 7 is taken as optimum for subsequent experiments.

Amperometric Detection of Nitrite. Furthermore, the detection of nitrite using the amperometry i-t technique was performed under optimal conditions. Figure 8A shows the amperometric response of the modified electrode with the successive addition of nitrite in pH 7 PBS. A steady state in the

https://dx.doi.org/10.1021/acsomega.0c02594
ACS Omega 2020, 5, 32160−32170

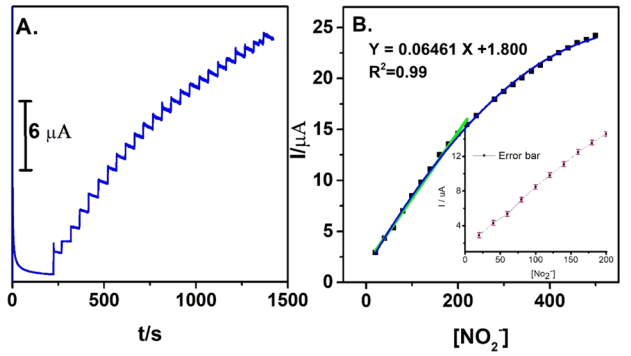

Figure 8. Amperometric responses for α-Fe_2O_3@MPC-chit modified screen-printed electrodes for successive addition of different concentrations of NO_2^- into the constantly stirred pH 7 PBS at an applied potential of +0.78 V vs Ag/AgCl (A) and their calibration plot of anodic peak current (I_{pa}) vs [NO_2^-] (B). Error bars denote standard deviation of three repeating measurements.

current response was obtained for each concentration within 3 s, which implies that the proposed sensor can catalyze nitrite at a faster rate which can be attributed from the porous structure of α-Fe_2O_3 nanoleaves and their synergistic effect with MPC-chit. The current response is linear with increasing concentration from 10 to 220 μM with a correlation coefficient of 0.999 (Figure 8B). The sensitivity and detection limit (S/N = 3) were found to be 0.913 μA μM^{-1} cm^{-2} and 31 nM, respectively. These observations indicate an excellent electrocatalytic performance of the modified electrode toward nitrite detection. The obtained results were compared with reported electrochemical sensors for nitrite detection. From the comparative Table 1, it can be concluded that the α-Fe_2O_3@MPC-chit modified electrode exhibits excellent analytical performance in terms of sensitivity, detection limit, and detection potential toward nitrite oxidation over many of the recently reported literature studies.[28−41]

Selectivity, Stability, Repeatability, and Reproducibility. The selectivity of the α-Fe_2O_3@MPC-chit modified electrode was investigated toward 20 μM nitrite in the presence of a 10-fold excess molar concentration of common interfering chemicals such as 0.2 mM $ZnCl_2$, $NiNO_3$, KCl, $CoCl_2$, Fe(II) acetate, $MgNO_3$, $CaCl_2$, $BaCl_2$, $NaNO_3$, $CdCl_2$, $PbCl_2$, and glucose pH 7 PBS at an applied potential of 0.78 V versus Ag/AgCl. As shown in Figure 9A, the amperometric

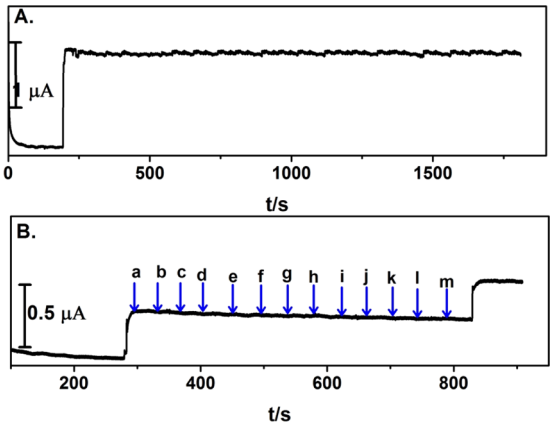

Figure 9. (A) Operational stability of the α-Fe_2O_3@MPC-chit modified screen printed electrode in the presence of 40 μM NO_2^- up to 1800 s. (B) Hydrodynamic amperometric responses for the α-Fe_2O_3@MPC-chit modified screen printed electrode for 20 μM NO_2^- (a) and 200 μM of $ZnCl_2$ (b), $NiNO_3$ (c), KCl (d), $CoCl_2$ (e), Fe(II) acetate (f), $MgNO_3$ (g), $CaCl_2$ (h), $BaCl_2$ (i), $NaNO_3$ (j), $CdCl_2$ (k), $PbCl_2$ (l), and glucose (m) into the constantly stirred pH 7 PBS at an applied potential of +0.78 V vs Ag/AgCl.

current signal was obtained only for nitrite, whereas no signals were found for the abovementioned interfering chemicals. This result suggests that the newly proposed modified electrode is highly selective for nitrite detection.

The long-term stability of the modified electrode toward nitrite detection is crucial for exploring it in real-time applications. Figure 9B shows the amperometric response of the modified electrode for 20 μM nitrite in constantly stirred

Table 1. Comparison of Analytical Parameters of Various Nitrite Sensors[a]

modified electrode	pH	Sensitivity	linear range	detection limit	detection potential (V)	technique	refs
CPEs-pHEMA-TBO	3	0.848 A M^{-1} cm^{-2}	1.0−1000 μM	1.6 μM	0.9	amp *i*−*t*	28
GNPs/graphene/MCE/GCE	4.75	0.47 A M^{-1} cm^{-2}	0.3−720 μM	0.1 μM	0.74	DPV	29
CG/PPy/Chit/GCE	4	0.381 A M^{-1} cm^{-2}	0.2−1000 μM	0.02 μM	0.876	DPV	30
$PrFeO_3$-MoS_2/GCE	4.5	0.327 A M^{-1} cm^{-2}	5−3 mM	1.67 μM	0.87	CV	31
GO-Mn_3O_4 microcubes/GCE	7	1.23 A M^{-1} cm^{-2}	0.1−1300 μM	0.02 μM	0.7	amp *i*−*t*	32
BC-GO/GCE	7	527.35 A M^{-1} cm^{-2}	0.5−4590 μM	0.2 μM	1.0	amp *i*−*t*	33
NPCF-GNs-GCE	9	3.1 A M^{-1} cm^{-2}	0.1−100 μM	88 nM	0.8	amp *i*−*t*	34
MOX/GCE	4	0.245 μA μM^{-1}	2−150 μM	0.22 μM	0.9	DPV	35
PdCoPC/GCE	6	0.01 μA μM^{-1}	0.2−40 μM	0.1 μM	0.86	amp *i*−*t*	36
rGO/MoS_2/GCE	7	0.46 A M^{-1} cm^{-2}	0.2−4800 μM	0.17 μM	0.8	amp *i*−*t*	37
Pt/$Ni(OH)_2$/MWCNT/GCE	7	0.145 A M^{-1} cm^{-2}	0.4−5670 μM	0.13 μM	0.75	amp *i*−*t*	38
graphite carbon ink/GCE		10.72 μA ppm^{-1}	4.35−47.83 μM	1.42 μM	0.96	SWV	39
CoNS/GO/PPy/GCE	8	0.519 A M^{-1} cm^{-2}	1.0−3167 μM	0.014 μM	0.8	amp *i*−*t*	40
PEDOT/PAS/GCE	7	0.13 A M^{-1} cm^{-2}	0.3−6594 μM	98 nM	0.8	amp *i*−*t*	41
A-Fe_2O@MPC-Chit/SPCE	7	0.913 A M^{-1} cm^{-2}	10−220 μM	31 nM	0.78	amp *i*−*t*	this work
		0.446 A M^{-1} cm^{-2}	0.5−12 mM			CV	

[a]pHEMA-poly(2-hydroxyethyl methacrylate); TBO-toluidine Blue; CPE-carbon paste electrode; GNPs-gold nanoparticles; MCE-mixed cellulose ester; CG-carboxyl graphene; PPy-polypyrrole; Chit-chitosan; GO-graphene oxide; BC-bacterial cellulose; NPCF-nanoporous Cu film; GNs-graphene nanosheets; MOG-Metal−organic xerogels; PPy-polypyrrole; PEDOT-poly(3,4-ethylenedioxythiophene); PAS-polyacenic semiconductor.

https://dx.doi.org/10.1021/acsomega.0c02594
ACS Omega 2020, 5, 32160−32170

pH 7 PBS. As shown in the Figure, the modified electrode retains almost its initial amperometric signal for 20 μM nitrite containing pH 7 PBS up to 1800 s. To investigate the reproducibility and repeatability of the modified electrode, the current responses of 1 mM nitrite for five independent modified electrodes and five successive detections of nitrite with one modified electrode were evaluated. The relative standard deviation of the obtained current signals is 4.2 and 3.3%, respectively. These observations indicate that the modified electrode has excellent operational stability, reproducibility, and repeatability toward nitrite detection.

Real Sample Analysis. To explore the practical suitability of the α-Fe_2O_3@MPC-chit modified electrode, the detection of nitrite in three different environmental samples such as tap water, industrial water, and drinking water was analyzed by an amperometric *i-t* method using a standard addition approach (Figure S5). A sample containing a known concentration of nitrite was spiked into constantly stirred pH 7 PBS. Other experimental conditions are the same as in Figure 8A. The results obtained using proposed methods were compared with those of the bench-top HPLC method, and the measurement results are given in Table 2. Appreciable recovery values in the range of 97 to 103.5% were obtained, which implies that the proposed sensor has practical applicability for sensing of nitrite in environmental samples.

Table 2. Determination of NO_2^- in Drinking Water, Industrial Water and Tap Water Using SPCE/α-Fe_2O_3@MPC-chit Using an Amp-It-Standard Addition Method and the Obtained Results were Compared with an HPLC Method

real samples	spiked (μM)	found[a] (μM)	found[a] (μM)	recovery[a] (%)	recovery[b] (%)
drinking water	20	19.8	19.67	99	98.3
	40	41.06	40.52	102.6	101.3
	60	62.1	59.23	103.5	98.71
	80	81.8	82.15	102.2	102.6
industrial water	20	19.4	9.85	97.0	99.25
	40	38.82	39.22	97.06	98.05
	60	61.91	62.15	103.1	103.5
	80	81.94	79.42	102.4	99.27
tap water	20	20.5	19.69	102.5	98.45
	40	39.50	40.60	98.7	101.5
	60	59.52	60.82	99.2	101.3
	80	80.60	79.62	100.7	99.5

[a]= electrochemical method. [b]= HPLC method.

Supercapacitor Application. To investigate the capacitance behavior of the as-prepared α-Fe_2O_3@MPC-chit composites, CV and galvanostatic charge−discharge studies were conducted in a three-electrode mode in the potential range from 0 to −0.9 V versus Hg/HgO in 3 M KOH. Figure 10A displays comparative cyclic voltammograms of Fe_2O_3 nanoleaves and the α-Fe_2O_3@MPC-chit modified electrode at a scan rate of 7 mV s^{-1}. The symmetric and rectangular with well-defined redox peak has appeared for both Fe_2O_3 nanoleaves and the α-Fe_2O_3@MPC-chit modified electrode, which implies the pseudocapacitive behavior of Fe_2O_3 nanoleaves. The intercalation and deintercalation of K^+ ions of the electrolyte within the cavity of Fe_2O_3 nanostructures is the possible reason for the pseudocapacitance of Fe_2O_3 nanoleaves. However, the area under the CV curve is quite larger for the α-Fe_2O_3@MPC-chit modified electrode than the Fe_2O_3 nanoleaves. This observation indicates that α-Fe_2O_3@MPC-chit nanocomposites have higher capacitances than Fe_2O_3 nanoleaves. Figure 10B displays the CV curves of the α-Fe_2O_3@MPC-chit modified electrode with different scan rates from 2−20 mV s^{-1} in 3 M KOH. The peak current increases linearly with the scan rate, which indicates the good capacitive behavior of the modified electrode. Moreover, the shape of the CV curves did not change significantly at different scan rates, suggesting that Fe_2O_3 nanoleaves retain good rate capability and reversibility. Figure 10C shows the galvanostatic charge−discharge studies of α-Fe_2O_3@MPC-chit composite at different current densities in the range of −0.9 to 0 V versus Hg/HgO. The specific capacitance of α-Fe_2O_3@MPC-chit nanocomposites was calculated to be 380.3 F g^{-1} at a current density of 1 A g^{-1} using eq 3. Furthermore, the composite can deliver a capacity of 350, 311, 279, 220, 189, and 154 F g^{-1} at a current density of 1.5, 2.0, 4.0, 6.0, 8.0, and 10.0 A g^{-1}, respectively. This decrement in the capacity at high current densities is likely due to a high IR drop and a slow rate of the α-Fe_2O_3 nanoleaves' redox reaction. However, the observed specific capacity of α-Fe_2O_3@MPC-chit nanocomposites is quite better than that of the previously reported Fe_2O_3 based electrodes[12−16,49−58] (Table 3). The high specific capacitance of the α-Fe_2O_3@MPC-chit composite is mainly attributed to the rational combination of the electrical double-layer capacitance of MPC-chit with the faradic capacitance of Fe_2O_3 nanoleaves. To investigate the α-Fe_2O_3@MPC-chit electrode for the practical energy storage applications, the long cycling performance was tested at a current density of 8.0 A g^{-1} in 3 M KOH solution. Figure 10D shows the plot of specific

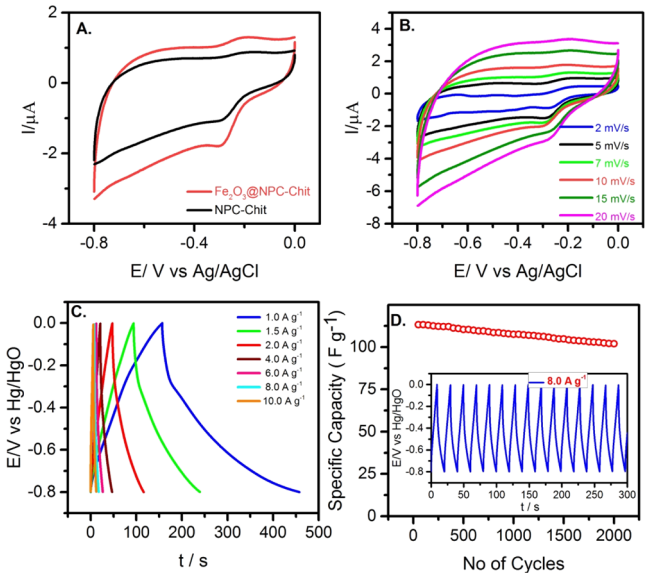

Figure 10. (A) CV responses for α-Fe_2O_3@MPC-chit and MPC-chit modified electrodes at a scan rate of 5 mV s^{-1}; (B) CV responses for different scan rates from 2−20 mV s^{-1} using α-Fe_2O_3@MPC-chit in 3 M KOH; (C) galvanostatic charge−discharge curves of the α-Fe_2O_3@MPC-chit modified electrode at different current densities at a potential range of 0 to −0.9 V vs Hg/HgO in 3 M aqueous KOH electrolyte; and (D) plot of capacitance retention of the α-Fe_2O_3@MPC-chit modified electrode vs number of cycles; inset shows charge−discharge profile of first few cycles at the current density of 8 A g^{-1}.

https://dx.doi.org/10.1021/acsomega.0c02594
ACS Omega 2020, 5, 32160−32170

Table 3. Electrochemical Performance of Reported Fe_2O_3-Based Materials in KOH Electrolytes[a]

Fe_2O_3 based material	electrolyte	potential range (V)	specific capacitance (F/g)	cycling stability	refs
Fe_2O_3 NDs@NG	2 M KOH	−1.0 to 0	274 at 1 A g^{-1}	81.8% after 50,000 cycles at 5 A g^{-1}	12
α-Fe_2O_3/rGO	1 M KOH	−1.0 to −0.3	903 at 1 A g^{-1}	70% after 1000 cycles at 5 A g^{-1}	13
N-rGO/α-Fe_2O_3	1 M KOH	−1.0 to 0	268.4 at 2 Ag^{-1}	95.8% after 2000 cycles at 3 A g^{-1}	14
α-Fe_2O_3 nanorods	6 M KOH	−1.2 to −0.5	300.5 at 1 A g^{-1}	64% after 2000 cycles at 5 A g^{-1}	15
Fe_2O_3-graphene	2 M KOH	−0.85 to 0	151.8 at 1 Ag^{-1}	86.0% after 2000 cycles at 2 A g^{-1}	16
α-Fe_2O_3 hollow nanoshuttles	1 M KOH	−1.0 to −0.5	175 at 1 A g^{-1}	93.6% after 2000 cycles at 8 A g^{-1}	49
Fe_2O_3/N-rGO	1 M KOH	−1.1 to −0.7	618 at 0.5 A g^{-1}	56.7% after 5000 cycles at 4 A g^{-1}	50
CL-GA/Fe_2O_3	3 M KOH	−1 to 0	445 at 1 A g1	89% after 5000 cycles	51
single-crystalline Fe2O_3 particles/graphene	1 M KOH	−1.05 to −0.3	908 at 2 A g^{-1}	75.0% after 200 cycles at 20 mV s^{-1}	52
3D Fe_2O_3/CCG	2 M KOH	−1.0 to 0.0	264 at 2.5 A g^{-1}	95.7% after 5000 cycles at 15.4 A g^{-1}	53
Fe_2O_3/rGOA	2 M KOH	−1.1 to 0.3	690 at 1 A g^{-1}	57% after 1500 cycles at 5 A g^{-1}	54
α-Fe_2O_3 thin film electrode	2 M KOH	−1.1 to 0.2	451 at 1 A g^{-1}	93.33% after 1000 cycles at 1 A g^{-1}	55
α-Fe_2O_3 nanorods	1 M KOH	0 to 0.4	601 at 1 A g^{-1}	86% after 1500 cycles at 4 A g^{-1}	56
GNS/Fe_2O_3	6 M KOH	−1.0 to −0.3	20 at 10 mA cm^{-2}	97% after 500 cycles at 10 mA cm^{-2}	57
Fe_2O_3 nanotubes/nitrogen-doped graphene	2 M KOH	−1 to 0	270 at 1 A g^{-1}	89% after 3000 cycles at 1 A g^{-1}	58
Fe_2O_3 nanoleaves @NPC-Chit	3 M KOH	−0.8 to 0	380 at 1 A g^{-1}	90.1% after 2000 cycles at 8 A g^{-1}	This work

[a]NDs-nanodots; NG-nitrogen doped graphene; CL-GA-cross-linked graphene aerogel; GNS-graphene nanosheet; CCG-chemically converted graphene; GOA-graphene oxide aerogel.

capacitance variation for α-Fe_2O_3@MPC-chit nanocomposites with a number of cycles. α-Fe_2O_3@MPC-chit retains 90.1% of its initial specific capacitance after 2000 cycles. This observation indicates that the fabricated electrode retains a high specific capacitance and good rate capability over the continuous cycles.

CONCLUSIONS

A simple hydrothermal method was adopted for synthesizing α-Fe_2O_3@MPC-chit nanocomposites and characterized by several physicochemical and electrochemical methods. By the exploitation of the excellent electrochemical property, the α-Fe_2O_3@MPC-chit nanocomposite was employed for dual applications: selective electrochemical nitrite sensors and supercapacitor applications. The fabricated sensor displayed several advantages including high sensitivity, wide linear range, low detection potential, good selectivity, and reproducibility. The excellent electrochemical activity can be attributed to the synergistic effect of Fe_2O_3 nanoleaves with MPC-chit. Overall, the proposed electrode displayed satisfactory analytical performance, which was proved by real-time detection of nitrite in environmental water samples. The hydrothermally synthesized α-Fe_2O_3@MPC-chit composite provided not only an improved nitrite sensor but also high-performance supercapacitors with excellent cyclic stability, which extends its application in both environmental sensors and energy storage devices.

EXPERIMENTAL SECTION

Reagents. Potassium ferricyanide and mesoporous carbon (MPC) were purchased from Aldrich. Cetyl trimethyl ammonium bromide (CTAB), potassium hydroxide, and potassium nitrite were obtained from Merck Life Science Pvt. Ltd, India. Other chemicals utilized in this investigation were all ACS-certified reagent grades and were employed without further purification. Deionized water was used for preparing stock solutions. The supporting electrolytes, namely, PBS (pH 7, 0.1 M) and potassium hydroxide (3 M) were used for nitrite detection and supercapacitor applications, respectively.

Instruments. An electrochemical workstation (VSP, Bio-Logic, France) was employed for all voltammetric and charge−discharge measurements. We have purchased a disposable screen-printed carbon electrode (SPCE) from Sinsil International, Bangalore. Electrochemical measurements were constructed using three-electrode systems which are SPCE (geometric area = 0.0707 cm^2), Ag/AgCl, and platinum wire as the working, reference, and auxiliary electrodes, respectively. The SPCE surface was electrochemically pretreated by carrying out CV at −0.2 to +1.0 V versus Ag/AgCl, at a scan rate of 50 mV s^{-1} for 10 continuous potential cycles in pH 7 PBS. Ultima Rikagu IV was used for generating XRD patterns. FT-IR studies were carried out using a Thermo Nicolet, model 6700. Confocal micro-Raman spectroscopy was performed using a Renishaw, model: RM 2000 instrument with an Ar^+ laser as the excitation source at a wavelength of 514 nm. Field-emission scanning electron microscope (FESEM) analysis was investigated using a Hitachi, model: S-3400N. The HPLC method was performed using Waters Alliance, model 2695 HPLC (Empower, version_3).

Synthesis of α-Fe_2O_3 Nanoleaves. A total of 0.5 M of $K_3[Fe(CN)_6]$ was prepared using 30 mL of double-distilled water under magnetic stirring. The concentration of surfactant CTAB added to the precursor solution was in a 1:2 ratio. The desired concentration of CTAB was added dropwise to the $K_3[Fe(CN)_6]$ solution under continuous stirring for 30 min. The solution mixture was transferred to an autoclave and subjected to hydrothermal treatment at 180 °C for 12 h. After the hydrothermal treatment, the autoclave was brought to room temperature. The precipitate thus obtained was washed with distilled water and ethanol multiple times to remove the impurities and excessive surfactant. The sample was dried at 100 °C for 12 h and finally subjected to calcination at 800 °C for 2 h, to produce Fe_2O_3 nanoleaves.

Preparation of the α-Fe_2O_3@MPC-chit Modified Screen-Printed Electrode. The α-Fe_2O_3@MPC-chit modified electrode was prepared by the simple drop-casting method. Before that, the chit solution was prepared as per the previous literature.[59] In brief, 50 mg of chit flakes were dissolved in 1% glacial acetic acid under magnetic stirring for 3

https://dx.doi.org/10.1021/acsomega.0c02594
ACS Omega 2020, 5, 32160−32170

Scheme 1. Hydrothermal Synthesis of α-Fe_2O_3 Nanoleaves and their Dual Applications: Selective Disposable Nitrite Sensor and High-Performance Supercapacitor

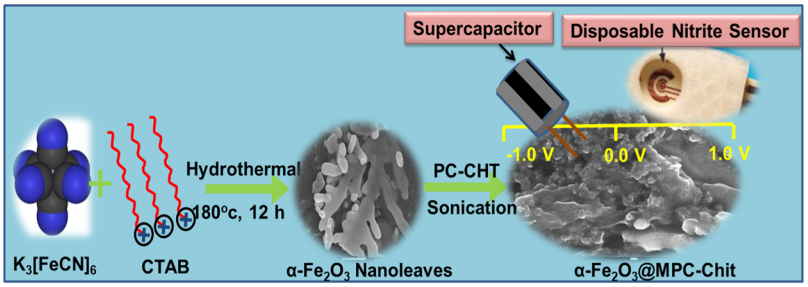

h. The pH of the synthesized chit solution was adjusted to 4−5 using NaOH solution. Then, 1 mg of MPC and 1 mg of α-Fe_2O_3 were dispersed in 1 mL of 0.5 wt % chit solution. A uniform black colloidal solution was obtained through ultrasonication at 1 hr. The modified electrode was prepared by drop-casting of 3 μL of a colloidal solution on the SPCE surface and drying to room temperature. After the process, the SPCE/α-Fe_2O_3@MPC-chit modified electrode was washed with deionized water to remove unbound composites and then used for electrochemical sensing application.

For supercapacitor applications, 15 μL of the prepared α-Fe_2O_3@MPC-chit solution was drop-casted on a precleaned stainless-steel (SS) electrode and then dried at 60 °C for 12 h. The electrochemical measurements were carried out in a three-electrode cell with an SS modified electrode as the working electrode, Hg/HgO as the reference electrode, and Pt foil as the counter electrode. The potential range for the galvanostatic charge−discharge studies and cyclic voltammograms was in the range of 0 to −0.9 V versus Hg/HgO in a 3 M KOH electrolyte. The specific capacitance of the α-Fe_2O_3@MPC-chit modified electrode was calculated using the following equation[60]

$$C = \frac{I\Delta t}{m\Delta V}(\mathrm{Fg}^{-1}) \quad (3)$$

where I is the discharge current (A), m indicates the mass of active materials (g), Δt is the discharge time (s), and ΔV is the potential window (V).

■ ASSOCIATED CONTENT

Supporting Information

The Supporting Information is available free of charge at https://pubs.acs.org/doi/10.1021/acsomega.0c02594.

UV, FT-IR, XRD, and Raman spectral responses of α-Fe_2O_3 Nanoleaves and amperometric i−t responses of the α-Fe_2O_3@MPC-chit modified screen printed electrode for NO_2^- detection in different water samples (PDF)

■ AUTHOR INFORMATION

Corresponding Authors

Palani Barathi − *Electrochemical Energy Research Lab, Centre for Nanoscience and Technology, Pondicherry University, Puducherry 605014, India; Department of Inorganic and Physical Chemistry, Indian Institute of Science, Bangalore 560012, India;* orcid.org/0000-0002-1157-7812; Email: barathianalytical@yahoo.co.in

Angaiah Subramania − *Electrochemical Energy Research Lab, Centre for Nanoscience and Technology, Pondicherry University, Puducherry 605014, India;* orcid.org/0000-0002-0855-752X; Email: a.subramania@gmail.com; Fax: +91-413-2655-348

Author

Anthonisamy Devaraj − *Department of Inorganic and Physical Chemistry, Indian Institute of Science, Bangalore 560012, India*

Complete contact information is available at: https://pubs.acs.org/10.1021/acsomega.0c02594

Notes

The authors declare no competing financial interest.

■ ACKNOWLEDGMENTS

P.B. gratefully thanks the Department of Science and Technology−Science and Engineering Research Board (DST-SERB), New Delhi, India, for providing the financial support under National Post-doctoral fellowship (N-PDF, PDF/2015/001004).

■ REFERENCES

(1) Niederberger, M.; Krumeich, F.; Hegetschweiler, K.; Nesper, R. An Iron Polyolate Complex as a Precursor for the Controlled Synthesis of Monodispersed Iron Oxide Colloids. *Chem. Mater.* **2002**, *14*, 78−82.

(2) Woo, K.; Lee, H. J.; Ahn, J.-P.; Park, Y. S. Sol−Gel Mediated Synthesis of Fe_2O_3 Nanorods. *Adv. Mater.* **2003**, *15*, 1761−1764.

(3) Guo, W.; Yang, Y.; Guo, Y.; Jia, Y.; Liu, H.; Guo, Y. Self-assembled hierarchical Bi12TiO20−graphene nanoarchitectures with excellent simulated sunlight photocatalytic activity. *Phys. Chem. Chem. Phys.* **2014**, *16*, 2705−2714.

(4) Jia, C.-J.; Sun, L.-D.; Yan, Z.-G.; You, L.-P.; Luo, F.; Han, X.-D.; Pang, Y.-C.; Zhang, Z.; Yan, C.-H. Single-Crystalline Iron Oxide Nanotubes. *Angew. Chem., Int. Ed.* **2005**, *44*, 4328−4333.

(5) Šutka, A.; Lagzdina, S.; Käämbre, T.; Pärna, R.; Kisand, V.; Kleperis, J.; Maiorov, M.; Kikas, A.; Kuusik, I.; Jakovlevs, D. Study of the structural phase transformation of iron oxide nanoparticles from an Fe2+ ion source by precipitation under various synthesis parameters and temperatures. *Mater. Chem. Phys.* **2015**, *149−150*, 473−479.

(6) Mitra, S.; Das, S.; Mandal, K.; Chaudhuri, S. Synthesis of a α-Fe2O3nanocrystal in its different morphological attributes: growth mechanism, optical and magnetic properties. *Nanotechnology* **2007**, *18*, 275608.

(7) Cui, X.; Liu, T.; Zhang, Z.; Wang, L.; Zuo, S.; Zhu, W. Hematite nanorods with tunable porous structure: Facile hydrothermal-calcination route synthesis, optical and photocatalytic properties. *Powder Technol.* **2014**, *266*, 113−119.

(8) Liu, X. Q.; Tao, S. W.; Shen, Y. S. Preparation and characterization of nanocrystalline α-Fe2O3 by a sol-gel process. *Sens. Actuators, B* **1997**, *40*, 161−165.

(9) Karade, V. C.; Parit, S. B.; Dawkar, V. V.; Devan, R. S.; Choudhary, R. J.; Kedge, V. V.; Pawar, N. V.; Kim, J. H.; Chougale, A. D. A green approach for the synthesis of α-Fe2O3 nanoparticles from Gardenia resinifera plant and it's In vitro hyperthermia application. *Heliyon* **2019**, *5*, No. e02044.
(10) Xu, B.; Zheng, D.; Qiu, W.; Gao, F.; Jiang, S.; Wang, Q. An ultrasensitive DNA biosensor based on covalent immobilization of probe DNA on fern leaf-like α-Fe2O3 and chitosan Hybrid film using terephthalaldehyde as arm-linker. *Biosens. Bioelectron.* **2015**, *72*, 175−181.
(11) Liu, L.; Wang, J.; Wang, C.; Wang, G. Facile synthesis of graphitic carbon nitride/nanostructured α-Fe2O3 composites and their excellent electrochemical performance for supercapacitor and enzyme-free glucose detection applications. *Appl. Surf. Sci.* **2016**, *390*, 303−310.
(12) Liu, L.; Lang, J.; Zhang, P.; Hu, B.; Yan, X. Facile Synthesis of Fe2O3 Nano-Dots@Nitrogen-Doped Graphene for Supercapacitor Electrode with Ultralong Cycle Life in KOH Electrolyte. *ACS Appl. Mater. Interfaces* **2016**, *8*, 9335−9344.
(13) Quan, H.; Cheng, B.; Xiao, Y.; Lei, S. One-pot synthesis of α-Fe2O3 nanoplates-reduced graphene oxide composites for supercapacitor application. *Chem. Eng. J.* **2016**, *286*, 165−173.
(14) Liu, H. D.; Zhang, J. L.; Xu, D. D.; Huang, L. H.; Tan, S. Z.; Mai, W. J. Easy one-step hydrothermal synthesis of nitrogen-doped reduced graphene oxide/iron oxide hybrid as efficient supercapacitor material. *J. Solid State Electrochem.* **2015**, *19*, 135−144.
(15) Li, J.; Zhang, W.; Zan, G.; Wu, Q. A high-performance dual-function material: self-assembled super long α-Fe2O3 hollow tubes with multiple heteroatom (C-, N- and S-) doping. *Dalton Trans.* **2016**, *45*, 12790−12799.
(16) Wang, D.; Li, Y.; Wang, Q.; Wang, T. Nanostructured Fe2O3−graphene composite as a novel electrode material for supercapacitors. *J. Solid State Electrochem.* **2012**, *16*, 2095−2102.
(17) Sravani, B.; Chandrashekar, Y.; Sri Chandana, P.; Maiyalagan, T.; Subramanyam Sarma, L. Bimetallic PtCu-decorated reduced graphene oxide (RGO)-TiO2 nanocomposite for efficient oxygen reduction reaction. *Synth. Met.* **2020**, *266*, 116433.
(18) Sravani, B.; Maseed, H.; Chandrasekhar, Y.; Veera Manohara Reddy, Y.; Srikanth, V. V. S. S.; Madhavi, G.; Subramanyam Sarma, L. A Pt-free graphenaceous composite as an electro-catalyst for efficient oxygen reduction reaction. *Nanoscale* **2019**, *11*, 13300−13308.
(19) Veera Manohara Reddy, Y.; Sravani, B.; Agarwal, S.; Gupta, V. K.; Madhavi, G. Electrochemical sensor for detection of uric acid in the presence of ascorbic acid and dopamine using the poly(DPA)/SiO2@Fe3O4 modified carbon paste electrode. *J. Electroanal. Chem.* **2018**, *820*, 168−175.
(20) Li, X.-R.; Kong, F.-Y.; Liu, J.; Liang, T.-M.; Xu, J.-J.; Chen, H.-Y. Synthesis of Potassium-Modified Graphene and Its Application in Nitrite-Selective Sensing. *Adv. Funct. Mater.* **2012**, *22*, 1981−1988.
(21) Mirvish, S. S. Role of N-nitroso compounds (NOC) and N-nitrosation in etiology of gastric, esophageal, nasopharyngeal and bladder cancer and contribution to cancer of known exposures to NOC. *Cancer Lett.* **1995**, *93*, 17−48.
(22) Aydın, A.; Ercan, Ö.O.; Taşcıoğlu, S. A novel method for the spectrophotometric determination of nitrite in water. *Talanta* **2005**, *66*, 1181−1186.
(23) Ferreira, I. M. P. L. V. O.; Silva, S. Quantification of residual nitrite and nitrate in ham by reverse-phase high performance liquid chromatography/diode array detector. *Talanta* **2008**, *74*, 1598−1602.
(24) Mikuška, P.; Večeřa, Z. Simultaneous determination of nitrite and nitrate in water by chemiluminescent flow-injection analysis. *Anal. Chim. Acta* **2003**, *495*, 225−232.
(25) Wang, X.; Adams, E.; Van Schepdael, A. A fast and sensitive method for the determination of nitrite in human plasma by capillary electrophoresis with fluorescence detection. *Talanta* **2012**, *97*, 142−144.
(26) Kalimuthu, P.; Abraham John, S. Highly sensitive and selective amperometric determination of nitrite using electropolymerized film of functionalized thiadiazole modified glassy carbon electrode. *Electrochem. Commun.* **2009**, *11*, 1065−1068.
(27) Kozub, B. R.; Rees, N. V.; Compton, R. G. Electrochemical determination of nitrite at a bare glassy carbon electrode; why chemically modify electrodes? *Sens. Actuators, B* **2010**, *143*, 539−546.
(28) Cimpean, M.-A.; Craciunescu, I.; Gligor, D. Amperometric sensor based on HEMA hydrogels modified with Toluidine Blue for nitrite detection in water samples. *Mater. Chem. Phys.* **2017**, *200*, 233−240.
(29) Wang, P.; Wang, M.; Zhou, F.; Yang, G.; Qu, L.; Miao, X. Development of a paper-based, inexpensive, and disposable electrochemical sensing platform for nitrite detection. *Electrochem. Commun.* **2017**, *81*, 74−78.
(30) Xiao, Q.; Feng, M.; Liu, Y.; Lu, S.; He, Y.; Huang, S. The graphene/polypyrrole/chitosan-modified glassy carbon electrode for electrochemical nitrite detection. *Ionics* **2018**, *24*, 845−859.
(31) Huang, H.; Lv, L.; Xu, F.; Liao, J.; Liu, S.; Wen, H.-r. PrFeO3-MoS2 nanosheets for use in enhanced electro-oxidative sensing of nitrite. *Microchim. Acta* **2017**, *184*, 4141−4149.
(32) Muthumariappan, A.; Govindasamy, M.; Chen, S.-M.; Sakthivel, K.; Mani, V. Screen-printed electrode modified with a composite prepared from graphene oxide nanosheets and Mn3O4 microcubes for ultrasensitive determination of nitrite. *Microchim. Acta* **2017**, *184*, 3625−3634.
(33) Zhang, Y.; Zhou, Z.; Wen, F.; Yuan, K.; Tan, J.; Zhang, Z.; Wang, H. Tubular structured bacterial cellulose-based nitrite sensor: preparation and environmental application. *J. Solid State Electrochem.* **2017**, *21*, 3649−3657.
(34) Majidi, M. R.; Ghaderi, S. Hydrogen bubble dynamic template fabrication of nanoporous Cu film supported by graphene nanaosheets: A highly sensitive sensor for detection of nitrite. *Talanta* **2017**, *175*, 21−29.
(35) Peng, Z. W.; Yuan, D.; Jiang, Z. W.; Li, Y. F. Novel metal-organic gels of bis(benzimidazole)-based ligands with copper(II) for electrochemical selectively sensing of nitrite. *Electrochim. Acta* **2017**, *238*, 1−8.
(36) Song, X.; Gao, L.; Li, Y.; Mao, L.; Yang, J.-H. A sensitive and selective electrochemical nitrite sensor based on a glassy carbon electrode modified with cobalt phthalocyanine-supported Pd nanoparticles. *Anal. Methods* **2017**, *9*, 3166−3171.
(37) Hu, J.; Zhang, J.; Zhao, Z.; Liu, J.; Shi, J.; Li, G.; Li, P.; Zhang, W.; Lian, K.; Zhuiykov, S. Synthesis and electrochemical properties of rGO-MoS2 heterostructures for highly sensitive nitrite detection. *Ionics* **2018**, *24*, 577−587.
(38) Sheng, Q.; Liu, D.; Zheng, J. A nonenzymatic electrochemical nitrite sensor based on Pt nanoparticles loaded Ni(OH)2/multi-walled carbon nanotubes nanocomposites. *J. Electroanal. Chem.* **2017**, *796*, 9−16.
(39) Petroni, J. M.; Lucca, B. G.; Ferreira, V. S. Simple and Inexpensive Electrochemical Platform Based on Novel Homemade Carbon Ink and its Analytical Application for Determination of Nitrite. *Electroanalysis* **2017**, *29*, 1762−1771.
(40) Wang, J.; Hui, N. A nanocomposite consisting of flower-like cobalt nanostructures, graphene oxide and polypyrrole for amperometric sensing of nitrite. *Microchim. Acta* **2017**, *184*, 2411−2418.
(41) Chen, L.; Liu, X.; Wang, C.; Lv, S.; Chen, C. Amperometric nitrite sensor based on a glassy carbon electrode modified with electrodeposited poly(3,4-ethylenedioxythiophene) doped with a polyacenic semiconductor. *Microchim. Acta* **2017**, *184*, 2073−2079.
(42) Zou, B.; Huang, W.; Han, M. Y.; Li, S. F. Y.; Xiaochun, W.; Zhang, Y.; Zhang, J.; Pengfei, W.; Wang, R. Anomalous optical properties and electron-phonon coupling enhancement in Fe2O3 nanoparticles coated with a layer of stearates. *J. Phys. Chem. Solids* **1997**, *58*, 1315−1320.
(43) Zhang, Z.; Hossain, M. F.; Takahashi, T. Fabrication of shape-controlled α-Fe2O3 nanostructures by sonoelectrochemical anodization for visible light photocatalytic application. *Mater. Lett.* **2010**, *64*, 435−438.

https://dx.doi.org/10.1021/acsomega.0c02594
ACS Omega 2020, 5, 32160−32170

(44) Bharathi, S.; Nataraj, D.; Seetha, M.; Mangalaraj, D.; Ponpandian, N.; Masuda, Y.; Senthil, K.; Yong, K. Controlled growth of single-crystalline, nanostructured dendrites and snowflakes of α-Fe2O3: influence of the surfactant on the morphology and investigation of morphology dependent magnetic properties. *CrystEngComm* **2010**, *12*, 373−382.
(45) Barathi, P.; Kumar, A. S. Facile Electrochemical Oxidation of Polyaromatic Hydrocarbons to Surface-Confined Redox-Active Quinone Species on a Multiwalled Carbon. *Nanotube Surface* **2013**, *19*, 2236−2241.
(46) García-Miranda Ferrari, A.; Foster, C. W.; Kelly, P. J.; Brownson, D. A. C.; Banks, C. E. Determination of the Electrochemical Area of Screen-Printed Electrochemical Sensing Platforms. *Biosensors* **2018**, *8*, 53.
(47) Bonanni, A.; Fernández-Cuesta, I.; Borrisé, X.; Pérez-Murano, F.; Alegret, S.; del Valle, M. DNA hybridization detection by electrochemical impedance spectroscopy using interdigitated gold nanoelectrodes. *Microchim. Acta* **2010**, *170*, 275−281.
(48) Laviron, E. Adsorption, autoinhibition and autocatalysis in polarography and in linear potential sweep voltammetry. *J. Electroanal. Chem. Interfacial Electrochem.* **1974**, *52*, 355−393.
(49) Zheng, X.; Yan, X.; Sun, Y.; Yu, Y.; Zhang, G.; Shen, Y.; Liang, Q.; Liao, Q.; Zhang, Y. Temperature-dependent electrochemical capacitive performance of the α-Fe2O3 hollow nanoshuttles as supercapacitor electrodes. *J. Colloid Interface Sci.* **2016**, *466*, 291−296.
(50) Ma, Z.; Huang, X.; Dou, S.; Wu, J.; Wang, S. One-Pot Synthesis of Fe2O3 Nanoparticles on Nitrogen-Doped Graphene as Advanced Supercapacitor Electrode Materials. *J. Phys. Chem. C* **2014**, *118*, 17231−17239.
(51) Gholipour-Ranjbar, H.; Ganjali, M. R.; Norouzi, P.; Naderi, H. R. Synthesis of cross-linked graphene aerogel/Fe2O3 nanocomposite with enhanced supercapacitive performance. *Ceram. Int.* **2016**, *42*, 12097−12104.
(52) Wang, H.; Xu, Z.; Yi, H.; Wei, H.; Guo, Z.; Wang, X. One-step preparation of single-crystalline Fe2O3 particles/graphene composite hydrogels as high performance anode materials for supercapacitors. *Nano Energy* **2014**, *7*, 86−96.
(53) Wu, J.; Zhou, A.; Huang, Z.; Li, L.; Bai, H. A Facile Method to Prepare Three-Dimensional Fe2O3/Graphene Composites as the Electrode Materials for Supercapacitors. *Chin. J. Chem.* **2016**, *34*, 67−72.
(54) Song, Z.; Liu, W.; Wei, W.; Quan, C.; Sun, N.; Zhou, Q.; Liu, G.; Wen, X. Preparation and electrochemical properties of Fe2O3/reduced graphene oxide aerogel (Fe2O3/rGOA) composites for supercapacitors. *J. Alloys Compd.* **2016**, *685*, 355−363.
(55) Yadav, A. A.; Deshmukh, T. B.; Deshmukh, R. V.; Patil, D. D.; Chavan, U. J. Electrochemical supercapacitive performance of Hematite α-Fe2O3 thin films prepared by spray pyrolysis from non-aqueous medium. *Thin Solid Films* **2016**, *616*, 351−358.
(56) Xu, X.; Cao, C.; Zhu, Y. Facile synthesis of single crystalline mesoporous hematite nanorods with enhanced supercapacitive performance. *Electrochim. Acta* **2015**, *155*, 257−262.
(57) Yang, W.; Gao, Z.; Wang, J.; Wang, B.; Liu, L. Hydrothermal synthesis of reduced graphene sheets/Fe2O3 nanorods composites and their enhanced electrochemical performance for supercapacitors. *Solid State Sci.* **2013**, *20*, 46−53.
(58) Cheng, T.; Li, W.; Yu, B.; He, M.; Cao, L.; Li, X.; Zheng, X.; Ren, Z. Facile synthesis of hollow Fe2O3 nanotubes on nitrogen-doped graphene and their electrochemical performances. *Ionics* **2017**, *23*, 3203−3210.
(59) Annamalai, S. K.; Palani, B.; Chandrasekara Pillai, K. Highly stable and redox active nano copper species stabilized functionalized-multiwalled carbon nanotube/chitosan modified electrode for efficient hydrogen peroxide detection. *Colloids Surf., A* **2012**, *395*, 207−216.
(60) Lin, T.-W.; Dai, C.-S.; Hung, K.-C. High Energy Density Asymmetric Supercapacitor Based on NiOOH/Ni3S2/3D Graphene and Fe3O4/Graphene Composite Electrodes. *Sci. Rep.* **2014**, *4*, 7274.

https://dx.doi.org/10.1021/acsomega.0c02594
ACS Omega 2020, 5, 32160−32170